Journal of Materials Chemistry A

Enhanced Thermoelectric Performance of the F4-TCNQ Doped FASnI3 Thin Films

Journal:	*Journal of Materials Chemistry A*
Manuscript ID	TA-ART-09-2020-009329.R1
Article Type:	Paper
Date Submitted by the Author:	09-Nov-2020
Complete List of Authors:	Zheng, Luyao; University of Akron, School of Polymer Science and Polymer Engineering Zhu, Tao; University of Akron, School of Polymer Science and Polymer Engineering Li, Yifan; University of Akron, Chemical and Biomolecular Engineering Wu, Haodong; University of Akron, School of Polymer Science and Polymer Engineering Yi, Chao; University of Akron, School of Polymer Science and Polymer Engineering Zhu, Jiahua; University of Akron, Chemical and Biomolecular Engineering Gong, Xiong; University of Akron, School of Polymer Science and Polymer Engineering

Enhanced Thermoelectric Performance of the F4-TCNQ Doped $FASnI_3$ Thin Films

Luyao Zheng,[1,#] Tao Zhu,[1,#] Yifan Li,[2,#] HaodongWu,[1] Chao Yi,[1] Jiahua Zhu,[2,*] Xiong Gong[1,*]
[1)]School of Polymer Science and Polymer Engineering and [2)]Department of Chemical and Bimolecular Engineering, College of Engineering and Polymer Science, The University of Akron, Akron, OH 44325, USA

ABSTRACT

In the past decade, great effects have been devoted to the development of organic-inorganic hybrid perovskites for approaching efficient photovoltaics, but fewer attention has been paid on their thermoelectric applications. In this study, for the first time, we report thermoelectric performance of the 2,3,5,6-tetrafluoro-7,7,8,8-tetracyanoquinodimethane (F4-TCNQ) doped $NH_2CHNH_2SnI_3$ ($FASnI_3$) thin films. It is found that the electrical conductivities of the F4-TCNQ doped $FASnI_3$ thin films are increased and then decreased along with increased doping levels of F4-TCNQ. Systematically studies indicate that enhanced electrical conductivities are attributed to the increased charge carrier concentrations and mobilities, and superior film morphologies of the F4-TCNQ doped $FASnI_3$ thin films, and decreased electrical conductivities are originated from the cracks and poor film morphology of the F4-TCNQ doped $FASnI_3$ thin films induced by excess F4-TCNQ dopants. The quantitative thermal conductivity scanning thermal microscopy studies reveal that the F4-TCNQ doped $FASnI_3$ thin films exhibit ultralow thermal conductivities. Moreover, the thermoelectric performance of the F4-TCNQ doped $FASnI_3$ thin films is investigated. It is found that the F4-TCNQ doped $FASnI_3$ thin films exhibit a Seebeck coefficient of ~310 $\mu V\ K^{-1}$, a power factor of ~ 130 $\mu W\ m^{-1}\ K^{-2}$ and a *ZT* value of ~0.19 at room temperature. All these results demonstrate that our studies open a door for exploring cost-effective less-toxic organic-inorganic hybrid perovskites in the application of heat-to-electricity conversion at room temperature.

# These authors are equally contributed to this work

* Corresponding authors, E-mails: xgong@uakron.edu (XG); jzhu1@uakron.edu (JZ); Fax: (330) 972 3406

1. Introduction

In the past decades, many effects have been devoted to the development of thermoelectric materials for converting heat into electricity.[1-9] The thermoelectric performance is evaluated by the dimensionless figure of merit, ZT, which is described as:[10,11]

$$ZT = \frac{\sigma S^2}{\kappa} T \qquad (1)$$

where σ is the electrical conductivity, S is the Seebeck coefficient, κ is thermal conductivity, and T is absolute temperature, respectively. Thus, semiconductors with high electrical conductivities but low thermal conductivities are ideally for approaching high thermoelectric performance. Many semiconductors have been intensively investigated.[12-27] It was reported that nanostructured GeTe, PbTe, PbS and SnTe alloys possess both high electrical conductivities and Seebeck coefficients, and high thermal conductivities as well.[22-27] Although the state-of-art inorganic thermoelectric materials could exhibit a *ZT* value over 1, their high-temperature processing restricts their practical applications. Whereas, organic semiconductors possess low thermal conductivities, but poor electrical conductivities and low Seebeck coefficients, consequently, low *ZT* values.[16-19]

In the recent decade, organic-inorganic hybrid perovskites with a typical formula of ABX_3 (where A is $CH_3NH_3^+$ (MA^+) or $NH_2CHNH_2^+$ (FA^+), or Cs, B is Pb^{2+} or Sn^{2+}, and X is Cl^-, or Br^-, or I^- or their combination), have been drawn greatest attention for approaching cost-effective efficient photovoltaics. However, fewer attention has been paid to its thermoelectric applications.[28-30] Studies indicated that hybrid perovskites possess the “electron-crystal phonon-glass” intrinsic and the phonon inhibiting structure.[31-35] As a result, hybrid perovskites possess not only superior optoelectronic properties, but also exhibit low thermal conductivities.[31-35] It was reported that Pb-based perovskites exhibited low electrical conductivities (10^{-7} S cm^{-1} to 10^{-4} S cm^{-1}), which was due to its low charge carrier concentrations ($<10^{17}$ cm^{-3}).[35-39] Sn-based perovskites exhibited relatively decent electrical conductivities ($\sim10^{-2}$ S cm^{-1}), which was ascribed to the substantial contribution of *s*-orbitals to the valance band maximum.[36,40,41] Moreover, the oxidation of Sn^{2+} to Sn^{4+} within Sn-based perovskites provides additional possibility for p-type self-doping, further improving its electronic properties.[42,43] Thus, Sn-based perovskites are good candidates for approaching high thermoelectric performance. A high electrical conductivity of 282 S cm^{-1}, a low thermal conductivity of 0.38 W m^{-1} K^{-1}, and with corresponding a ZT value of 0.11 at 320 K from $CsSnI_3$ nanowires were reported in 2017.[44] Later on, a ZT value of 0.14 at 345 K was observed from Cl-doped $CsSnI_{3-x}Cl_x$ thin film.[45] Recently, a ZT value of 0.123 at 473 K from stable $CsS_{1-x}Ge_xI_3$ alloy bulk crystals was reported.[46] However, the thermoelectric performance of organic-inorganic hybrid Sn-based perovskites was rarely reported.[36,47]

In this study, we first report dramatically enhanced electrical conductivities of 2, 3, 5, 6-tetrafluoro-7, 7, 8, 8-tetracyanoquinodimethane (F4-TCNQ) doped $FASnI_3$ thin films. It is found that the electrical conductivities of the F4-TCNQ doped $FASnI_3$ thin films are increased and then decreased along with increased doping levels of F4-TCNQ. Systematically studies indicate that enhanced electrical conductivities are attributed to the increased charge carrier concentrations and mobilities, and superior film morphologies of the resultant the F4-TCNQ doped $FASnI_3$ thin films, and decreased electrical conductivities are originated from the cracks and poor film morphology of the F4-TCNQ doped $FASnI_3$ thin films induced by excess F4-TCNQ dopants. We then report ultralow thermal conductivities of the F4-TCNQ doped $FASnI_3$ thin films, which are investigated by a quantitative thermal conductivity scanning thermal microscopy (SThM). Afterward, we, for the first time, report thermoelectric performance of the F4-TCNQ doped $FASnI_3$ thin films. At room temperature, the F4-TCNQ doped $FASnI_3$ thin films exhibit a Seebeck coefficient of ~310 μV K^{-1}, a power factor of 130 μW m^{-1} K^{-2} and a ZT value of 0.19.

2. Experimental section

2.1 Materials

Tin (II) iodide (SnI_2, ultra-dry, 99.999%, metals basis) and molybdenum (VI) oxide (MoO_3, 99.95%, metals basis) were purchased from Alfa Aesar. Formamidinium iodide (FAI) was purchased from Greatcell Solar. F4-TCNQ (97%), fullerene (C_{60}, 99.5%), anhydrous N, N-dimethylformamide (DMF), dimethyl sulfoxide (DMSO), toluene (99.8%) were purchased from Sigma-Aldrich. Poly(3,4-ethylenedioxythiophene):polystyrene sulfonate (PEDOT:PSS, Clevios PH1000) was purchased from Heraeus Precious Metals North America. All chemicals were used as received without further purification.

2.2 Preparation of the F4-TCNQ doped $FASnI_3$ thin films

The F4-TCNQ $FASnI_3$ thin films were prepared through deposition of precursor solution (both 1M FAI and SnI_2 were dissolved in a DMF:DMSO (4: 1 in volume) mixed solvent, with different concentrations of F4-TCNQ (0.01, 0.05, 0.075, and 0.1 mg/mL) by spin-coating method. The spin coating was divided into two parts: firstly, the precursor solution was dripped onto substrates and the substrates started to spin at 5000 rpm with acceleration of 1000 r s^{-2} for 20 second (s); secondly, 250 μL toluene was dripped onto the wet thin films and then spin coating was kept for another 20 s at 5000 rpm to remove the solvents. No further thermal annealing treatment was applied.

2.3 Characterizations of the F4-TCNQ doped $FASnI_3$ thin films

For X-ray spectroscopy (XPS) measurement, both pristine $FASnI_3$ thin film and the F4-TCNQ doped $FASnI_3$ thin films were deposited on glass substrates. The top ~ 50 nm thick layer was etched off to reveal the elemental information in the bulk rather than surface. XPS was conducted on a PHI 5000 Versa Probe II scanning XPS microprobe. The X-ray diffraction (XRD) was performed by Rigaku SmartLab X-Ray Diffractometer. The electrical conductivities of both pristine $FASnI_3$ thin film and the F4-TCNQ doped $FASnI_3$ thin films were measured by the four-probe set up based on van der Pauw method.[48] Two Keithley 2400 were utilized to measure the current-voltage (I-V) curves and calculate the average resistance through 8 values among the four probes. The thickness of pristine $FASnI_3$ thin film and the F4-TCNQ doped $FASnI_3$ thin films were measured by the DektakXT surface profile measuring system. The dielectric constants of perovskite thin films were measured by the capacitance-frequency characteristics using Keithley model 82-WIN Simultaneous CF System. The capacitance-voltage (C-V) measurements were carried out on a HP 4194A impedance/gain-phase analyzer under dark condition, with an oscillating voltage of 10 mV under 10 kHz. The hole-only diode, ITO/PEDOT:PSS/$FASnI_3$ (or F4-TCNQ doped $FASnI_3$)/MoO_3/Ag diodes, where ITO is indium doped tin oxide and Ag is silver, is utilized for the C-V measurement to calculate the charge carrier concentrations. Above hole-only diode is also used to estimate the hole mobility. The electron-only diode, ITO/C_{60}/$FASnI_3$ (F4-TCNQ doped $FASnI_3$)/C_{60}/Al, where Al is aluminum, is used to estimate the electron mobility. The charge carrier mobilities are estimated from the current densities versus voltages (J-V*)* characteristics conducted in dark, based on the space charge limited current (SCLC) method. The top view scanning electron microscopy (SEM) images were obtained by using a field emission scanning electron microscope (JEOL-7401).

Thermal conductivities were characterized by the scanning thermal microscopy (SThM) model, which was performed by Park System XE7 atomic force microscope (AFM). Pristine $FASnI_3$ thin film and the F4-TCNQ doped $FASnI_3$ thin films were deposited on glass substrates. The thermal tip is thermally grown on SiO_2 cantilever which was made of silicon base. Base dimension is 2×3 mm^2 and cantilever dimension is $150 \times 60 \times 1$ μm^3. The resistor metal is made of 5 nm NiCr and 40 nm Pd. Tip height is 12 μm and tip radius is ~100 nm. The resistance of the tip is around 200-600 Ω. Thermal coefficient of resistivity is about 1 $\Omega/^{o}C$. Spring constant is 0.45 N/m and resonance frequency is 48 KHz. The pre-setting probe current was 1.20 mA. Micro-hardness was characterized by force-displacement (F-D) method with AFM. Thermal probe was used to collect the F-D data that ensures the captured current signal and measured micro-hardness are from exactly the same region. The micro-hardness results were further analyzed by Olive and Pharr model. Surface roughness was analyzed from surface topography. Slope value was determined by the calculation of line profile via AFM original images without flatting process. AFM was conducted by Atomic Park System XE7 AFM. The Seebeck coefficients were measured by two Peltier devices, which were connected with two LFI3000 wavelength temperature controllers to generate a temperature gradient (ΔT) of 10K. The characteristics of thermoelectric parameters and the C-V and SCLC measurements were conducted in glovebox with N_2 atmosphere at room temperature.

3. Results and discussion

The electrical conductivity of pristine $FASnI_3$ thin film was reported to be 1.72×10^{-2} S cm^{-1}, which was originated from its low charge carrier concentrations.[41,49] In order to approach high thermoelectric performance, the electrical conductivity of $FASnI_3$ thin film needs to be boosted.[50] Towards the end, F4-TCNQ is introduced into $FASnI_3$ thin films since F4-TCNQ was widely used to boost the electrical conductivities of organic materials.[51-55] The preparation of the F4-TCNQ doped $FASnI_3$ thin films is described in **Experimental section**.

XPS is first carried out to verify whether F4-TCNQ is indeed doped into $FASnI_3$ or not. **Fig. 1** presents high resolution XPS spectra of pristine $FASnI_3$ thin film and the F4-TCNQ doped $FASnI_3$ thin films. As compared with pristine $FASnI_3$ thin films, the appearance of F *1s* orbital features in the F4-TCNQ doped $FASnI_3$ thin films indicates the presence of F4-TCNQ within $FASnI_3$ thin films (**Fig. 1a**). As indicated in **Fig. 1b**, both "=NH", and "$-NH_2$" function groups are observed from $FASnI_3$ thin films. The binding energies (BEs) of 398.0 eV and 397.5 eV, for "=NH" and "$-NH_2$" function groups, respectively, are observed from pristine $FASnI_3$ thin film. Whereas, the corresponding BEs are 398.8 eV and 396.7 eV, respectively, for the F4-TCNQ doped $FASnI_3$ thin films. Such BEs shifts indicate that hydrogen bonds of '=NH…F' and '-NH_2…F' are formed in the F4-TCNQ doped $FASnI_3$ thin films.[56] Moreover, the BEs of 495.1 eV and 486.8 eV, corresponding to the Sn $3d_{3/2}$ and Sn $3d_{5/2}$ spin-orbitals, respectively, are observed from pristine $FASnI_3$ thin film.[31,41,] Whereas the corresponding BEs of 495.9 eV and 487.5 eV are observed from the F4-TCNQ doped $FASnI_3$ thin films (**Fig. 1c**). Furthermore, the BEs of 628.6 eV and 617.1 eV, corresponding to the I $3d_{3/2}$ and I $3d_{5/2}$ spin-orbitals, respectively, are observed from pristine $FASnI_3$ thin film, Whereas the corresponding BEs of 629.1 eV and 617.6 eV, respectively, are observed from the F4-TCNQ doped $FASnI_3$ thin films (**Fig. 1d**). Such large BEs shifts demonstrate that both oxidation states and chemical environments of Sn and I are dramatically different in the F4-TCNQ doped $FASnI_3$ thin films compared to those in pristine $FASnI_3$ thin films. All these results demonstrate that F4-TCNQ is indeed doped into $FASnI_3$ thin films.

The XRD patterns of pristine $FASnI_3$ and the F4-TCNQ doped $FASnI_3$ thin films are displayed in **Supporting Information 1, (SI 1**). It is found that both prisinte $FASnI_3$ and F4-TCNQ doped $FASnI_3$ thin films possess the cubic $Pm\bar{3}m$ space group at room temperature.[57] The full width at half maximum (FWHM) of the (111) peak for F4-TCNQ doped $FASnI_3$ thin film is 1.21^o, which is smaller than that (1.96^o) for pristine $FASnI_3$ thin film, indicating that the F4-TCNQ doped $FASnI_3$ thin film possesses an optimal crystalline feature.

The atomic weight concentrations of element F and Sn are calculated based on the full XPS spectra (**SI 2**). Thus, the doping levels (a molar ratio of F4-TCNQ to $FASnI_3$) in the F4-TCNQ doped $FASnI_3$ thin films are further calculated. For example, as the doping concentration of F4-TCNQ is at 0.01 mg/mL, the doping level of F4-TCNQ within the F4-TCNQ doped $FASnI_3$ thin film is 1.94%. Correspondingly, the doping levels are 3.85%, 5.78% and 8.79% for the F4-TCNQ concentrations of 0.05 mg/mL, 0.075 mg/mL and 0.10 mg/mL, respectively.

The electrical conductivities of the F4-TCNQ doped $FASnI_3$ thin films versus the doping levels of F4-TCNQ are shown in **Fig. 2a.** The electrical conductivity of pristine $FASnI_3$ thin film prepared from a precursor solution without SnF_2 additives is 2.81 S cm^{-1}. This electrical conductivity is two orders of magnitude higher than reported value (1.72×10^{-2} S cm^{-1}) from pristine $FASnI_3$ thin film prepared from a precursor solution with SnF_2 additives.[41,49] SnF_2 additives could restrict Sn^{2+} to be oxidized to Sn^{4+}, resulting in stable $FASnI_3$ thin film, but with poor electrical conductivity.[41,49] The electrical conductivity of the F4-TCNQ doped $FASnI_3$ thin film is dramatically enhanced to 11.03 S cm^{-1} as the doping level of F4-TCNQ is at 1.94%. Moreover, the electrical conductivity of the F4-TCNQ doped $FASnI_3$ thin film as the doping level of F4-TCNQ at 3.85% is enhanced to 13.65 S cm^{-1}. Such enhanced electrical conductivity is approximatively 5 times higher than that of pristine $FASnI_3$ thin film prepared without SnF_2

additives and 800 times higher than that prepared with SnF_2 additives. However, the electrical conductivities of the F4-TCNQ doped $FASnI_3$ thin films as the doping levels at 5.78% and 8.79% are dropped to 6.22 S cm^{-1} and 1.12 S cm^{-1}, respectively.

The electrical conductivity (σ) is described as,[58]

$$\sigma = qn\mu \qquad (2)$$

where q is the elementary charge, n is the charge carrier concentration and μ is the charge carrier mobility, respectively. In order to understand the correlation between the electrical conductivities and the doping levels, the charge carrier concentrations (n) of the F4-TCNQ doped $FASnI_3$ thin films are calculated based on the capacitance-voltage measurement (**SI 3**), according to the Mott-Schottky model.[59-61] **Fig. 2b** presents the charge carrier concentrations of the F4-TCNQ doped $FASnI_3$ thin films versus of the doping levels of F4-TCNQ. The charge carrier concentration of pristine $FASnI_3$ thin film is calculated to be 3.2×10^{19} cm^{-3}, which is consistent with reported one.[41] The charge carrier concentration of 6.7×10^{19} cm^{-3} is observed from the F4-TCNQ doped $FASnI_3$ thin film as the doping level of F4-TCNQ at 1.94%. The charge carrier concentration is dramatically increased to 2.7×10^{20} cm^{-3} for the F4-TCNQ doped $FASnI_3$ thin film as the doping level of F4-TCNQ at 3.85%. However, as the doping levels of F4-TCNQ is increased to over 5.78%, the charge carrier concentrations of the resultant F4-TCNQ doped $FASnI_3$ thin films are decreased. Thus, the F4-TCNQ doped $FASnI_3$ thin films exhibit enhanced and then decreased electrical conductivities.

On the other hand, the charge carrier mobilities are calculated based on the space charge limited current method, according to the Mott-Gurney law (**SI 4**).[59-61] **Fig. 2b** also shows the charge carrier mobilities of the F4-TCNQ doped $FASnI_3$ thin films versus the doping levels of F4-TCNQ. Noted the thickness of F4-TCNQ doped $FASnI_3$ thin films with doping levels of 0%, 1.94%, 3.85%, 5.78% and 8.79% are ~ 272 nm, ~ 265 nm, ~ 253 nm, ~ 228 nm and ~ 221 nm, respectively. For pristine $FASnI_3$ thin film, the electron and hole mobilities are 6.80×10^{-5} cm^2 V^{-1} s^{-1} and 2.63×10^{-4} cm^2 V^{-1} s^{-1}, respectively, which are consistent with reported ones.[62] The electron and hole mobilities of 5.69×10^{-5} cm^2 V^{-1} s^{-1} and 7.08×10^{-4} cm^2 V^{-1} s^{-1}, respectively, are observed from the F4-TCNQ doped $FASnI_3$ thin film as the doping level of F4-TCNQ at 1.94%. Moreover, the electron and hole mobilities of 1.85×10^{-4} cm^2 V^{-1} s^{-1} and 2.19×10^{-3} cm^2 V^{-1} s^{-1}, respectively, are observed from the F4-TCNQ doped $FASnI_3$ thin film as the doping level of F4-TCNQ at 3.85%. However, the electron and hole mobilities are decreased to 7.22×10^{-5} cm^2 V^{-1} s^{-1} and 1.64×10^{-3} cm^2 V^{-1} s^{-1}, respectively, for the F4-TCNQ doped $FASnI_3$ thin film as the doping level of F4-TCNQ at 5.78%. The electron and hole mobilities are further dropped to 9.88×10^{-6} cm^2 V^{-1} s^{-1} and 9.33×10^{-4} cm^2 V^{-1} s^{-1}, respectively, for the F4-TCNQ doped $FASnI_3$ thin film as the doping level of F4-TCNQ at 8.79%. Thus, the F4-TCNQ doped $FASnI_3$ thin films exhibit enhanced and then decreased electrical conductivities since the F4-TCNQ doped $FASnI_3$ thin films possess increased and decreased charge carrier mobilities along with increased doping levels of F4-TCNQ.

To understand decreased charge carrier mobilities, thus reduced electrical conductivities of the F4-TCNQ doped $FASnI_3$ thin films with high doping levels of F4-TCNQ, SEM is carried out to study film morphologies of the resultant F4-TCNQ doped $FASnI_3$ thin films. **Fig. 3a-e** displays the top-view SEM images of the F4-TCNQ doped $FASnI_3$ thin films. Pristine $FASnI_3$ thin film possesses many pinholes, with a domain size of ~280 nm (**Fig. 3a**). Whereas, the pinholes are nearly diminished and the domain sizes are enlarged to ~320 nm and ~345 nm for the F4-TCNQ doped $FASnI_3$ thin films as the doping levels of F4-TCNQ at 1.94% and 3.85%, respectively (**Fig. 3b, c**). Such superior film morphologies and enlarged domain sizes could facilitate charge carrier to be efficiently transported, resulting in enlarged charge carrier mobilities.[63] As a result, enhanced electrical conductivities are observed from the F4-TCNQ doped $FASnI_3$ thin films. However, as indicated in **Fig. 3d, e**, the F4-TCNQ doped $FASnI_3$ thin films as the doping levels of F4-TCNQ at 5.78% and 8.79% possess poor film morphologies with obvious cracks, which could restrict charge carrier to be efficiently transported, resulting in poor charge carrier mobilities. As a result, the F4-TCNQ doped $FASnI_3$ thin films with high doping levels of F4-TCNQ possess poor electrical conductivity.

The thermal conductivities of $MAPbX_3$ (X=Cl, Br, I) crystals were theoretically reported,[31,32,34] but its experimental values were rarely reported.[64] Since micro-thermal and macro-thermal resistances should be considered as film thickness are increased to hundreds of nanometers[65] and organic-inorganic hybrid perovskites are similar to polymers, in this study, the thermal conductivities of the F4-TCNQ doped $FASnI_3$ thin films are investigated through a quantitative thermal conductivity SThM method (**SI 5**), which was used for polymers.[66] The thermal conductivity (κ) is described as:

$$\kappa = \frac{(I-B)\left(\frac{1}{4a}+\frac{H\gamma}{\pi F m}+\frac{1}{\pi r_0}\right)}{A} \qquad (3)$$

where I is the probe current, H is the micro-hardness, γ is the effective roughness, F is the contact force (5.97 nN), m is the effective slope between the tip and the sample, a is the tip radius (100 nm), r_0 is the radius of the heat source (100 nm), A and B are the model constants, respectively. Different to previously computational simulations,[31,44,67-70] all these parameters are obtained through experimental results. Furthermore, $MAPbI_3$ thin films are tested to validate the

SThM model (**SI 5**). The thermal conductivity of $MAPbI_3$ thin film is measured to be 0.5 W m^{-1} K^{-1}, which is consistent with reported value.[31,34] Thus, A of 2.4173×10^4 K V^{-1} and B of 1.1969 mA are used to calculate the thermal conductivities of the F4-TCNQ doped $FASnI_3$ thin films. H, γ, m and I these parameters for the F4-TCNQ doped $FASnI_3$ thin films are listed in **Table S2** (**SI 5**).

Fig. 4a-e presents the probe current mappings of pristine $FASnI_3$ thin film and the F4-TCNQ doped $FASnI_3$ thin films. The average probe current for pristine $FASnI_3$ thin film is 1.20234±0.00054 mA; whereas the average probe currents are 1.20303±0.00044 mA, 1.20469±0.00096 mA, 1.20500±0.00099 mA and 1.20778±0.00147 mA for the F4-TCNQ doped $FASnI_3$ thin films as the doping levels of F4-TCNQ at 1.94%, 3.85%, 5.78% and 8.79%, respectively. Thus, based on the SThM model, the thermal conductivities of the F4-TCNQ doped $FASnI_3$ thin films are calculated and the results are shown in **Fig. 4f**. The thermal conductivity of pristine $FASnI_3$ thin film is 0.141±0.014 W m^{-1} K^{-1}. To the best of our knowledge, this is the first time reported the thermal conductivity of $FASnI_3$ thin film. The thermal conductivities are increased to 0.167±0.012W m^{-1} K^{-1}, 0.212±0.026 W m^{-1} K^{-1}, 0.219±0.027 W m^{-1} K^{-1} and 0.289±0.039 W m^{-1} K^{-1} for the F4-TCNQ doped $FASnI_3$ thin films as the doping levels of F4-TCNQ at 1.94%, 3.85%, 5.78% and 8.79%, respectively. As compared with pristine $FASnI_3$ thin film, slightly enhancement in the thermal conductivities of the F4-TCNQ doped $FASnI_3$ thin films along with increased doping levels is attributed to the electron-contribution effect.[71] Moreover, a high thermal conductivity observed from the F4-TCNQ doped $FASnI_3$ thin film as the doping level of F4-TCNQ at 8.79% is probably originated from large leakage probe current induced by poor film morphology. But nevertheless, the thermal conductivities of both pristine

$FASnI_3$ thin film and the F4-TCNQ doped $FASnI_3$ thin films are lower than those from nanostructured GeTe (~5.5-6.3 W m^{-1} K^{-1}), PbTe (~2.0-3.2 W m^{-1} K^{-1}), PbS (~1.1-2.5 W m^{-1} K^{-1}) and SnTe (~3.9-8.9 W m^{-1} K^{-1}),[22-27] and even smaller than those of organic semiconductors (~ 0.5 W m^{-1} K^{-1}) at room temperature.[16-18]

To understand film morphology affects the probe current, thus the thermal conductivity, AFM is carried out to investigate the surface roughness of thin films. **Fig. 5** displays AFM images of pristine $FASnI_3$ thin film and the F4-TCNQ doped $FASnI_3$ thin films. The effective surface roughness of pristine $FASnI_3$ thin film is estimated to be ~ 69 nm, whereas, the effective surface roughness of ~ 59 nm, ~ 47 nm, ~ 57 nm and ~ 77 nm are observed for the F4-TCNQ doped $FASnI_3$ thin films as the doping levels of F4-TCNQ at 1.94%, 3.85%, 5.78% and 8.79%, respectively. Such rough surface could generate leakage current, leading a relatively enlarged probed current. As a result, enlarged thermal conductivities are observed from the F4-TCNQ doped $FASnI_3$ thin films as the doping level at 8.79%.

The thermoelectric performance of the F4-TCNQ doped $FASnI_3$ thin films is firstly evaluated by the Seebeck coefficient (S), which is described by:[50]

$$S = \frac{8\pi^2 {k_B}^2}{3qh^2} m^* T\left(\frac{\pi}{3n}\right)^{\frac{2}{3}} \qquad (4)$$

where k_B is the Boltzmann constant, q is the elementary charge, h is the Planck constant, m^* is the effective mass, T is the temperature, and n is the charge carrier density. **Fig. 6a** presents the Seebeck coefficients of the F4-TCNQ doped $FASnI_3$ thin films versus the doping levels of F4-TCNQ. A positive Seebeck coefficient of ~213 μV K^{-1} is observed from pristine $FASnI_3$ thin film. The Seebeck coefficient observed from $FASnI_3$ thin film prepared in the absence of SnF_2 additives is smaller than the one with SnF_2 additives.[49] Such difference is attributed to the exist of Sn^{4+}, which could induce p-type self-doping, generating higher charge carrier concentration,[72,73] consequently resulting in smaller Seebeck coefficient.[50] The Seebeck coefficient of the F4-TCNQ doped $FASnI_3$ thin film as the doping level of F4-TCNQ at 1.94% is slightly increased to ~244 μV K^{-1}. The best Seebeck coefficient of ~310 μV K^{-1} is observed from the F4-TCNQ doped $FASnI_3$ thin film as the doping level of F4-TCNQ at 3.85%. Such enhanced Seebeck coefficients are probably originated from increased narrow bands with high density of state at the Fermi surface.[50] But, the Seebeck coefficients of the $FASnI_3$ thin films as the doping levels of at 5.78% and 8.79% are dropped to ~256 μV K^{-1} and ~218 μV K^{-1}, respectively. These decreased Seebeck coefficients are probably due to inferior film morphology of highly F4-TCNQ doped $FASnI_3$ thin films.

The power factor (PF) is another parameter used to evaluate the thermoelectric performance.[50] *PF* is described as:[50]

$$PF = \sigma S^2 \qquad (5)$$

where σ is the electrical conductivity, S is the Seebeck coefficient. Pristine $FASnI_3$ thin film possesses a *PF* of 12.75 μW m^{-1} K^{-2}; whereas, the F4-TCNQ doped $FASnI_3$ thin films as the doping levels at 1.94% and 3.85% possess *PF*s of 65.69 μW m^{-1} K^{-2} and 131.18 μW m^{-1} K^{-2}, respectively. Such high *PF* values are attributed to the improved electrical conductivities and Seebeck coefficients. However, *PF* value is decreased to 40.78 μW m^{-1} K^{-2} for the F4-TCNQ doped $FASnI_3$ thin film as the F4-TCNQ doping level at 5.78%. *PF* is dramatically dropped to 5.34 μW m^{-1} K^{-2} for the F4-TCNQ doped $FASnI_3$ thin film as the F4-TCNQ doping level at 8.79%. These reduced *PF* values are probably attributed to poor electrical conductivities of the F4-TCNQ doped $FASnI_3$ thin films.

The dimensionless figure of merit, *ZT*, is also studied. **Fig. 6b** presents the *ZT* values of the F4-TCNQ doped $FASnI_3$ thin films versus the doping levels of F4-TCNQ at room temperature (T=298 K). Pristine $FASnI_3$ thin film shows a *ZT* value of 0.03. To the best of our knowledge, this is the first reported experimental *ZT* value for Sn-based perovskites. *ZT* values are increased to 0.12 and 0.19 for the F4-TCNQ doped $FASnI_3$ thin films as the F4-TCNQ doping levels are at 1.94% and 3.85%, respectively. Such enhanced *ZT* values are ascribed to the increased electrical conductivities of the F4-TCNQ doped $FASnI_3$ thin films. However, *ZT* values are decreased to 0.06 and 0.01 for the F4-TCNQ doped $FASnI_3$ thin films as the F4-TCNQ doping levels are at 5.78% and 8.79%, respectively. These decreased *ZT* values are attributed to poor electrical conductivities of the F4-TCNQ doped $FASnI_3$ thin films.

4. Conclusion

In summary, for the first time, we reported the thermoelectric performance of the F4-TCNQ doped $FASnI_3$ thin films. In order to enhance the thermoelectric performance of $FASnI_3$ thin films, F4-TCNQ was used to dope $FASnI_3$ thin films. Systematically studies indicated that the enhanced electrical conductivities of the F4-TCNQ dope $FASnI_3$ thin films are attributed to its increased charge carrier concentrations and mobilities, as well as its superior film morphologies, and decreased electrical conductivities are due to poor film morphology of the F4-TCNQ dope $FASnI_3$ thin films induced by excess F4-TCNQ dopants. After that, we quantitatively calculated the thermal conductivities of the F4-TCNQ doped $FASnI_3$ thin films based on the SThM method. It was found that F4-TCNQ doped Sn-based perovskite thin films exhibited ultralow thermal conductivity. Furthermore, the thermoelectric performances including Seebeck coefficient, power factors and *ZT* values of the F4-TCNQ doped $FASnI_3$ thin films were investigated. At room temperature, a Seebeck coefficient of ~310 μV K^{-1}, a power factor of 130 μW m^{-1} K^{-2} and a *ZT* value of 0.19 were observed from the F4-TCNQ doped $FASnI_3$ thin films. All these results indicated that we provided a facile and simple approach to realize enhanced thermoelectric performance from cost-effective less-toxic organic-inorganic hybrid perovskite materials.

Acknowledgments

The authors acknowledge the National Science Foundation (NSF) (ECCS/EPMD1903303) and Air Force Office of Scientific Research (AFOSR) (through the Organic Materials Chemistry Program, Grant Number: FA9550-15-1-0292, Program Manager, Dr. Kenneth Caster) for financial supports.

Conflict of interest

There are no conflicts to declare.

Keywords

Thermoelectric performance, organic-inorganic hybrid perovskites, doping effect, electrical conductivity, thermal conductivity

References

1. C. Uher, *Materials Aspect of Thermoelectricity*, CRC press, 2016.
2. J. Mao, H. Zhu, Z. Ding, Z. Liu, G. A. Gamage, G. Chen and Z. Ren, *Science*, 2019, **365**, 495-498. DOI:10.1126/science.aax7792.
3. D. Zhao and G. Tan, *Appl. Therm. Eng.*, 2014, **66**, 15-24. DOI:10.1016/j.applthermaleng.2014.01.074.
4. N. Wang, L. Han, H. He, N.-H. Park and K. Koumoto, *Energy Environ. Sci.*, 2011, **4**, 3676-3679. DOI:10.1039/C1EE01646F.
5. Z. Liu, B. Sun, X. Liu, J. Han, H. Ye, Y. Tu, C. Chen, T. Shi, Z. Tang and G. Liao, *J. Mater. Chem. A*, 2018, **6**, 7409-7419. DOI:10.1039/C8TA00526E.
6. L. Xu, Y. Xiong, A. Mei, Y. Hu, Y. Rong, Y. Zhou, B. Hu and H. Han, *Adv. Energy Mater.*, 2018, **8**, 1702937. DOI:10.1002/aenm.201702937.
7. S. L. Kim, J.-H. Hsu and C. Yu, *Nano Energy*, 2018, **48**, 582-589. DOI:10.1016/j.nanoen.2018.04.015.
8. A. Härtel, M. Janssen, D. Weingarth, V. Presser and R. van Roij, *Energy Environ. Sci.*, 2015, **8**, 2396-2401. DOI:10.1039/C5EE01192B.
9. Y. Dai, R. Wang and L. Ni, *Renew. Energy*, 2003, **28**, 949-959. DOI:10.1016/S0960-1481(02)00055-1.
10. R. R. Heikes and R. W. Ure, *Thermoelectricity: science and engineering*, Interscience Publishers, 1961.
11. T. Power, *Thermoelectrics Handbook: Macro to Nano*, 2005.
12. D. M. Rowe, *Thermoelectrics handbook: macro to nano*, CRC press, 2018.

13. R. Ure Jr and R. Heikes, *Theoretical calculation of device performance*, Interscience Publishers, Inc.: New York, NY, USA, 1961.

14. F. Rosi, *Solid-State Electron.*, 1968, **11**, 833-868. DOI:10.1016/0038-1101(68)90104-4Get.

15. F. Rosi, E. Hockings and N. Lindenblad, *RCA Rev. (US)*, 1961, **22**.

16. W. Shi, T. Deng, G. Wu, K. Hippalgaonkar, J. S. Wang and S. W. Yang, *Adv. Mater.*, 2019, **31**, 1901956. DOI:10.1002/adma.201901956.

17. G.-H. Kim, L. Shao, K. Zhang and K. P. Pipe, *Nat. Mater.*, 2013, **12**, 719-723. DOI:10.1038/nmat3635.

18. Y. Hiroshige, M. Ookawa and N. Toshima, *Synth. Met.*, 2007, **157**, 467-474. DOI:10.1016/j.synthmet.2007.05.003.

19. Y. Xuan, X. Liu, S. Desbief, P. Leclère, M. Fahlman, R. Lazzaroni, M. Berggren, J. Cornil, D. Emin and X. Crispin, *Phys. Rev. B*, 2010, **82**, 115454. DOI:10.1103/PhysRevB.82.115454.

20. O. Bubnova, Z. U. Khan, A. Malti, S. Braun, M. Fahlman, M. Berggren and X. Crispin, *Nat. Mater.*, 2011, **10**, 429. DOI:10.1038/nmat3012.

21. J. Feng-Xing, X. Jing-Kun, L. Bao-Yang, X. Yu, H. Rong-Jin and L. Lai-Feng, *Chin. Phys. Lett.*, 2008, **25**, 2202. DOI:10.1088/0256-307X/25/6/076.

22. J. Dong, F.-H. Sun, H. Tang, J. Pei, H.-L. Zhuang, H.-H. Hu, B.-P. Zhang, Y. Pan and J.-F. Li, *Energy Environ. Sci.*, 2019, **12**, 1396-1403. DOI:10.1039/C9EE00317G.

23. K. Biswas, J. He, I. D. Blum, C.-I. Wu, T. P. Hogan, D. N. Seidman, V. P. Dravid and M. G. Kanatzidis, *Nature*, 2012, **489**, 414. DOI:10.1038/nature11439.

24. Y. Xiao and L.-D. Zhao, *npj Quantum Mater.*, 2018, **3**, 55. DOI:10.1038/s41535-018-0127-y.
25. L.-D. Zhao, J. He, S. Hao, C.-I. Wu, T. P. Hogan, C. Wolverton, V. P. Dravid and M. G. Kanatzidis, *J. Am. Chem. Soc.*, 2012, **134**, 16327-16336. DOI:10.1021/ja306527n.
26. Q. Zhang, B. Liao, Y. Lan, K. Lukas, W. Liu, K. Esfarjani, C. Opeil, D. Broido, G. Chen and Z. Ren, *Proc. Natl. Acad. Sci.*, 2013, **110**, 13261-13266. DOI:10.1073/pnas.1305735110.
27. G. Tan, F. Shi, S. Hao, H. Chi, L.-D. Zhao, C. Uher, C. Wolverton, V. P. Dravid and M. G. Kanatzidis, *J. Am. Chem. Soc.*, 2015, **137**, 5100-5112. DOI:10.1021/jacs.5b00837.
28. A. Kojima, K. Teshima, Y. Shirai and T. Miyasaka, *J. Am. Chem. Soc.*, 2009, **131**, 6050-6051. DOI:10.1021/ja809598r.
29. M. Grätzel, *Acc. Chem. Res.*, 2017, **50**, 487-491. DOI:10.1021/acs.accounts.6b00492.
30. J.-P. Correa-Baena, M. Saliba, T. Buonassisi, M. Grätzel, A. Abate, W. Tress and A. Hagfeldt, *Science*, 2017, **358**, 739-744. DOI:10.1126/science.aam6323.
31. A. Pisoni, J. Jacimovic, O. S. Barisic, M. Spina, R. Gaál, L. Forró and E. Horváth, *J. Phys. Chem. Lett.*, 2014, **5**, 2488-2492. DOI:10.1021/acs.jpcc.5b03939.
32. C. Ge, M. Hu, P. Wu, Q. Tan, Z. Chen, Y. Wang, J. Shi and J. Feng, *J. Phys. Chem. C*, 2018, **122**, 15973-15978. DOI:10.1021/acs.jpcc.8b05919.
33. T. Hata, G. Giorgi and K. Yamashita, *Nano Lett.*, 2016, **16**, 2749-2753. DOI:10.1021/acs.nanolett.6b00457.
34. X. Mettan, R. Pisoni, P. Matus, A. Pisoni, J. i. Jaćimović, B. Náfrádi, M. Spina, D. Pavuna, L. Forró and E. Horváth, *J. Phys. Chem. C*, 2015, **119**, 11506-11510. DOI:10.1021/acs.jpcc.5b03939.

35. M. A. Haque, M. I. Nugraha, S. H. K. Paleti and D. Baran, *J. Phys. Chem. C*, 2019, **123**, 14928-14933. DOI:10.1021/acs.jpcc.9b02830.

36. C. C. Stoumpos, C. D. Malliakas and M. G. Kanatzidis, *Inorg. Chem.*, 2013, **52**, 9019-9038. DOI:10.1021/ic401215x.

37. D. Shi, V. Adinolfi, R. Comin, M. Yuan, E. Alarousu, A. Buin, Y. Chen, S. Hoogland, A. Rothenberger and K. Katsiev, *Science*, 2015, **347**, 519-522. DOI:10.1126/science.aaa2725.

38. Q. Dong, Y. Fang, Y. Shao, P. Mulligan, J. Qiu, L. Cao and J. Huang, *Science*, 2015, **347**, 967-970. DOI: 10.1126/science.aaa5760.

39. C. Wehrenfennig, G. E. Eperon, M. B. Johnston, H. J. Snaith and L. M. Herz, *Adv. Mater.*, 2014, **26**, 1584-1589. DOI:10.1002/adma.201305172.

40. Y. He and G. Galli, *Chem. of Mater.*, 2014, **26**, 5394-5400. DOI:10.1021/cm5026766.

41. W. Liao, D. Zhao, Y. Yu, C. R. Grice, C. Wang, A. J. Cimaroli, P. Schulz, W. Meng, K. Zhu and R. G. Xiong, *Adv. Mater.*, 2016, **28**, 9333-9340. DOI:10.1002/adma.201602992.

42. Y. Takahashi, H. Hasegawa, Y. Takahashi and T. Inabe, *J. Solid State Chem.*, 2013, **205**, 39-43. DOI:10.1016/j.jssc.2013.07.008.

43. I. Chung, J.-H. Song, J. Im, J. Androulakis, C. D. Malliakas, H. Li, A. J. Freeman, J. T. Kenney and M. G. Kanatzidis, *J. Am. Chem. Soc.*, 2012, **134**, 8579-8587. DOI:10.1021/ja301539s.

44. W. Lee, H. Li, A. B. Wong, D. Zhang, M. Lai, Y. Yu, Q. Kong, E. Lin, J. J. Urban and J. C. Grossman, *Proc. Natl. Acad. Sci.*, 2017, **114**, 8693-8697. DOI:10.1073/pnas.1711744114.

45. T. Liu, X. Zhao, J. Li, Z. Liu, F. Liscio, S. Milita, B. C. Schroeder and O. Fenwick, *Nat. Commun.*, 2019, **10**, 1-9. DOI:10.1038/s41467-019-13773-3.

46. F. Qian, M. Hu, J. Gong, C. Ge, Y. Zhou, J. Guo, M. Chen, Z. Ge, N. P. Padture and Y. Zhou, *J. Phys. Chem. C*, 2020, 124, 11749-11753. DOI:10.1021/acs.jpcc.0c00459.

47. L. Yan, M. Wang, C. Zhai, L. Zhao and S. Lin, *ACS Appl. Mater. Interfaces*, 2020, **12**, 40453-40464. DOI:10.1021/acsami.0c07501.

48. O. Philips'Gloeilampenfabrieken, *Philips Res. Rep*, 1958, **13**, 1-9.

49. S. Shao, J. Liu, G. Portale, H. H. Fang, G. R. Blake, G. H. ten Brink, L. J. A. Koster and M. A. Loi, *Adv. Energy Mater.*, 2018, **8**, 1702019. DOI:10.1002/aenm.201702019.

50. V. Dusastre, *Materials for sustainable energy: a collection of peer-reviewed research and review articles from Nature Publishing Group*, World Scientific, 2011.

51. T. Takenobu, T. Takano, M. Shiraishi, Y. Murakami, M. Ata, H. Kataura, Y. Achiba and Y. Iwasa, *Nat. Mater.*, 2003, **2**, 683-688. DOI:10.1038/nmat976.

52. T. Takenobu, T. Kanbara, N. Akima, T. Takahashi, M. Shiraishi, K. Tsukagoshi, H. Kataura, Y. Aoyagi and Y. Iwasa, *Adv. Mater.*, 2005, **17**, 2430-2434. DOI:10.1002/adma.200500759.

53. W. Chen, S. Chen, D. C. Qi, X. Y. Gao and A. T. S. Wee, *J. Am. Chem. Soc.*, 2007, **129**, 10418-10422. DOI:10.1021/ja071658g.

54. Q. Wang, C. Bi and J. Huang, *Nano Energy*, 2015, **15**, 275-280. DOI:10.1016/j.nanoen.2015.04.029.

55. J. E. Cochran, M. J. Junk, A. M. Glaudell, P. L. Miller, J. S. Cowart, M. F. Toney, C. J. Hawker, B. F. Chmelka and M. L. Chabinyc, *Macromolecules*, 2014, **47**, 6836-6846. DOI:10.1021/ma501547h.

56. S. Kerber, J. Bruckner, K. Wozniak, S. Seal, S. Hardcastle and T. Barr, *J. Vac. Sci. Technol. A: Vac., Surf., Films*, 1996, **14**, 1314-1320. DOI:10.1116/1.579947.

57. Y. Dang, Y.Zhou, X. Liu, D. Ju, S. Xia, H. Xia, X. Tao, *Angew. Chem. Int. Ed.,* 2016, **55**, 3447-3450. DOI: 10.1002/anie.201511792.

58. H. Goldsmid, *Proceedings of the Physical Society*, 1958, **71**, 633.

59. D. K. Schroder, *Semiconductor material and device characterization*, John Wiley & Sons, 2015.

60. R. H. Bube, *J. Appl. Phys.*, 1962, **33**, 1733-1737. DOI:10.1063/1.1728818.

61. P. Murgatroyd, *J. Phys. D: Appl. Phys.*, 1970, **3**, 151.

62. W. Gao, C. Ran, J. Li, H. Dong, B. Jiao, L. Zhang, X. Lan, X. Hou and Z. Wu, *J. Phys. Chem. Lett.*, 2018, **9**, 6999-7006. DOI:10.1021/acs.jpclett.8b03194.

63. C. Liu, Z. Huang, X. Hu, X. Meng, L. Huang, J. Xiong, L. Tan and Y. Chen, *ACS Appl. Mater. Interfaces*, 2018, **10**, 1909-1916. DOI:10.1021/acsami.7b15031.

64. R. Heiderhoff, T. Haeger, N. Pourdavoud, T. Hu, M. Al-Khafaji, A. Mayer, Y. Chen, H.-C. Scheer and T. Riedl, *The J. Phys. Chem. C*, 2017, **121**, 28306-28311. DOI:10.1021/acs.jpcc.7b11495.

65. M. Bahrami, M. M. Yovanovich, J. R. Culham, J. Thermophys Heat Transfer 18 (2004) 318-325. M. Bahrami, M. M. Yovanovich and J. R. Culham, *J. Thermophys. Heat Transfer*, 2004, **18**, 318-325.

66. Y. Li, N. Mehra, T. Ji and J. Zhu, *Nanoscale Horizons*, 2018, **3**, 505-516. DOI:10.1039/C8NH00043C.

67. Y. Liu, X. Li, J. Wang, L. Xu and B. Hu, *J. Mater. Chem. A*, 2017, **5**, 13834-13841. DOI:10.1039/C7TA03015K.

68. J. Callaway, *Physical Review*, 1959, **113**, 1046.

69. J. Callaway, *Physical Review*, 1961, **122**, 787.

70. G. A. Slack, in *Solid state physics*, Elsevier, 1979, vol. 34, 1-71.

71. G. J. Snyder and E. S. Toberer, in *materials for sustainable energy: a collection of peer-reviewed research and review articles from Nature Publishing Group*, World Scientific, 2011, 101-110.

72. M. H. Kumar, S. Dharani, W. L. Leong, P. P. Boix, R. R. Prabhakar, T. Baikie, C. Shi, H. Ding, R. Ramesh and M. Asta, *Adv. Mater.*, 2014, **26**, 7122-7127. DOI:10.1002/adma.201401991.

73. S. J. Lee, S. S. Shin, Y. C. Kim, D. Kim, T. K. Ahn, J. H. Noh, J. Seo and S. I. Seok, *J. Am. Chem. Soc.*, 2016, **138**, 3974-3977. DOI:10.1021/jacs.6b00142.

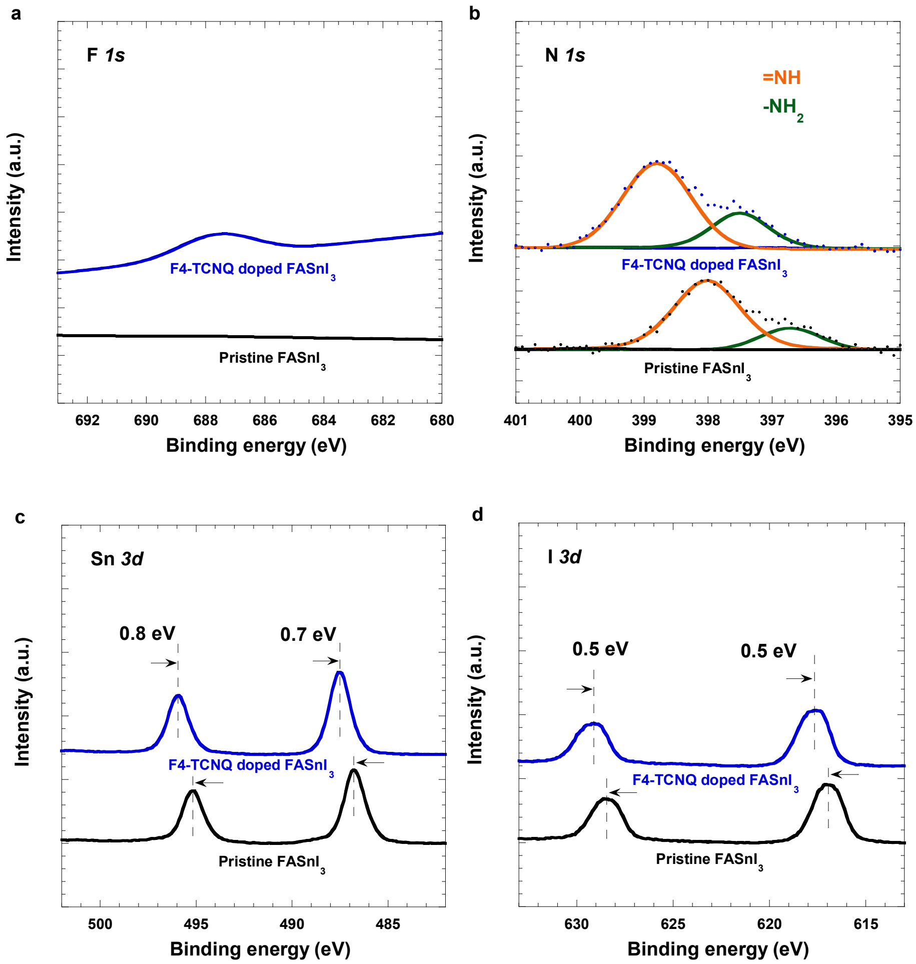

Fig. 1. XPS spectra of pristine $FASnI_3$ thin film (black) and the F4-TCNQ doped $FASnI_3$ thin film (blue), a) F 1*s*, b) N 1*s*, c) Sn 3*d*, and d) I 3*d* spin-orbitals.

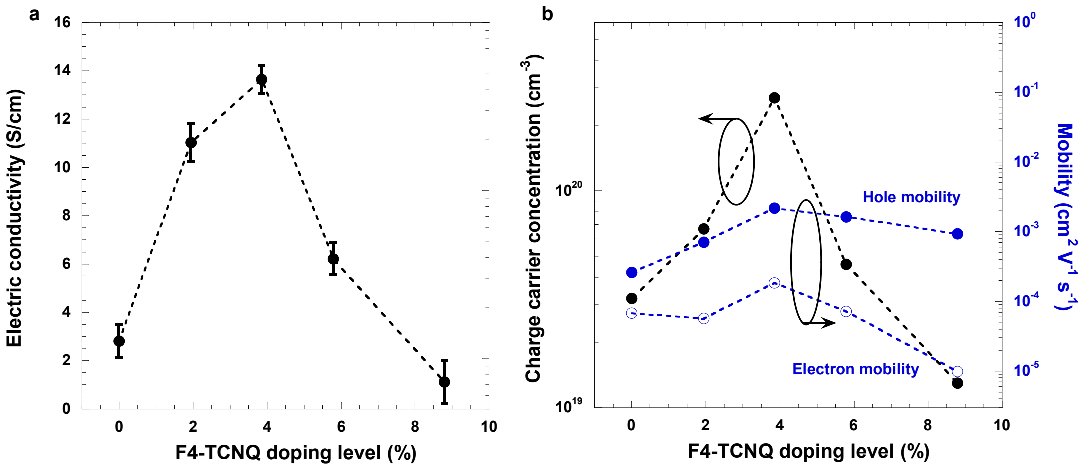

Fig. 2. a) The electrical conductivities of the F4-TCNQ doped $FASnI_3$ thin films versus of the doping levels of F4-TCNQ; b) The charge carrier concentration and the electron and hole mobilities of the F4-TCNQ doped $FASnI_3$ thin films versus of the doping levels of F4-TCNQ.

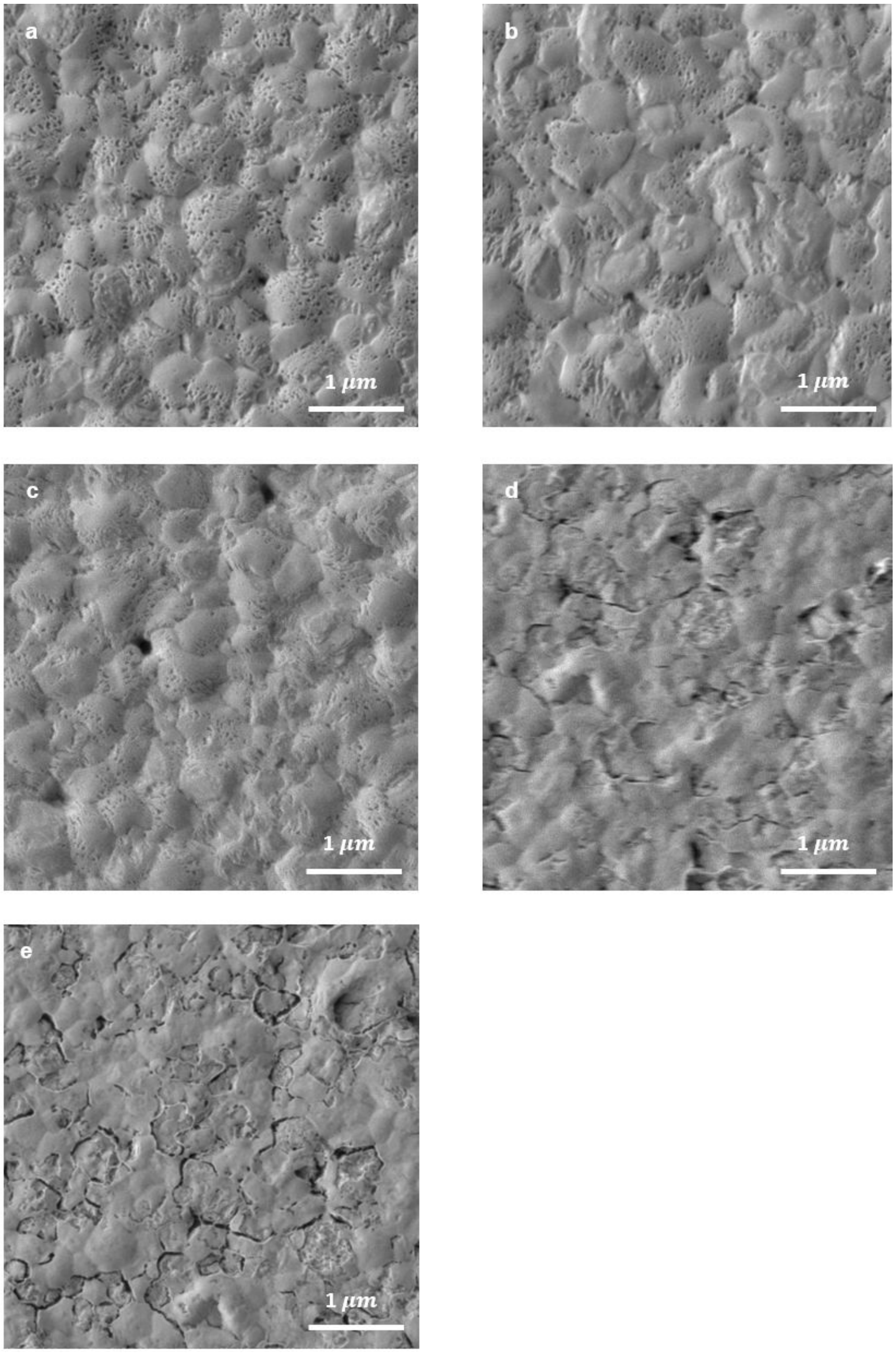

Fig. 3. Top-view SEM images of a) pristine $FASnI_3$ thin film, and the TCNQ-doped $FASnI_3$ thin films as the doping levels of b) 1.94%, c) with 3.85%, d) 5.78% and e) with 8.79%, respectively.

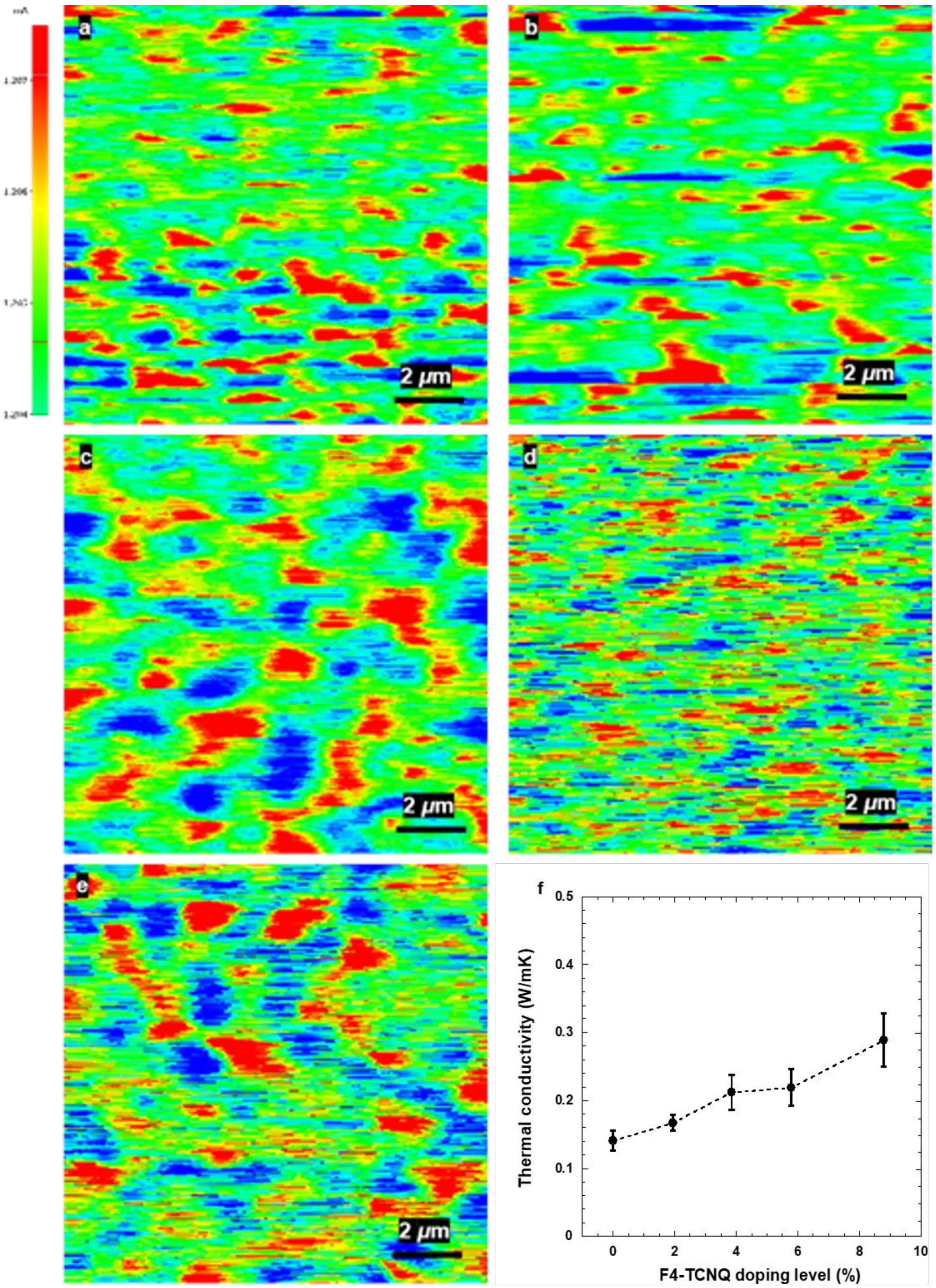

Fig. 4. The probe current mappings of a) pristine $FASnI_3$ thin films, and the TCNQ-doped $FASnI_3$ thin films as the doping levels of b) 1.94%, c) with 3.85%, d) 5.78% and e) with 8.79%, respectively, and f) the thermal conductivities of the F4-TCNQ doped $FASnI_3$ thin films versus the doping levels of F4-TCNQ.

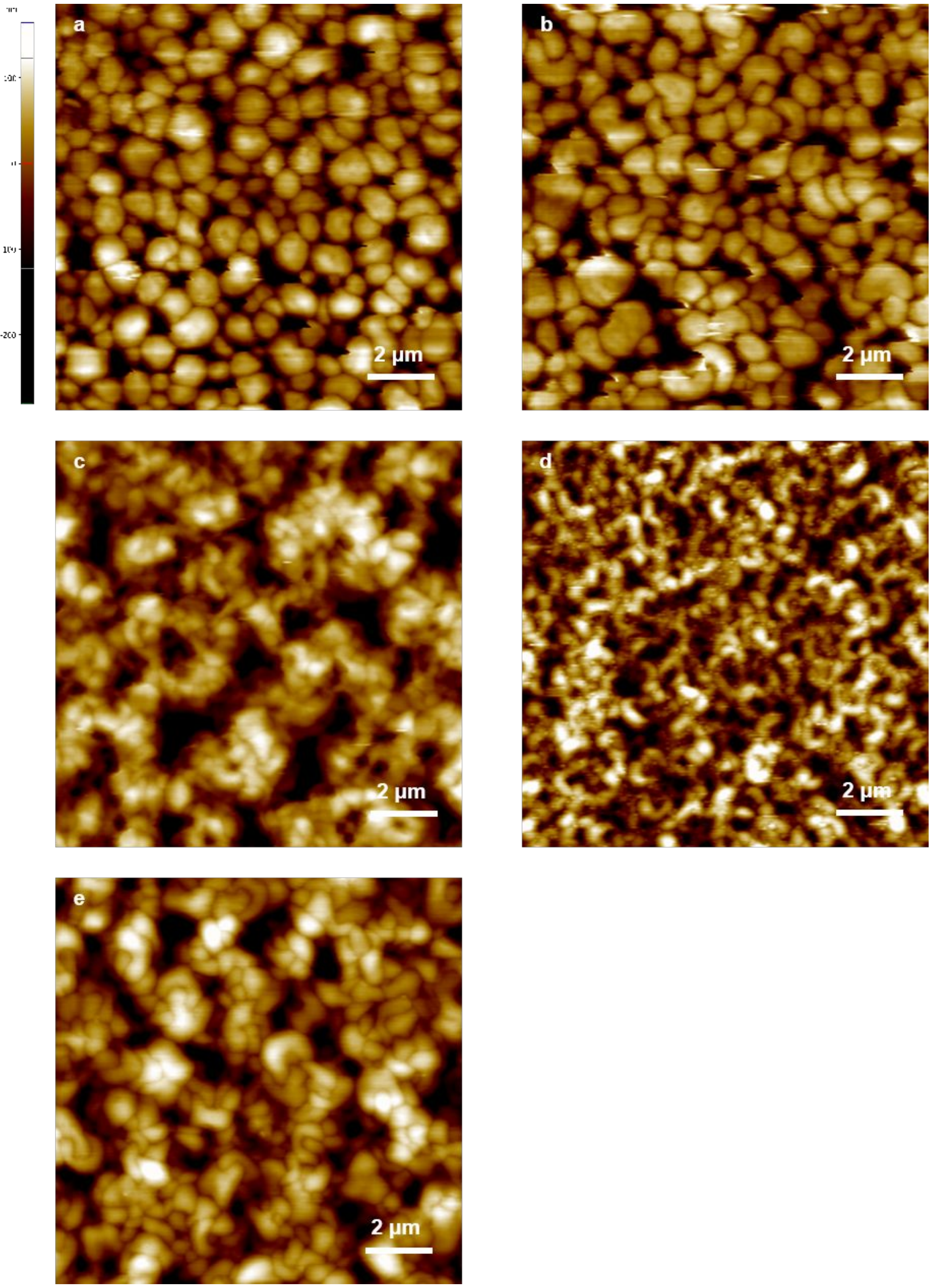

Fig. 5. AFM images of a) pristine $FASnI_3$ thin film and the F4-TCNQ doped $FASnI_3$ thin films as the doping levels at b) 1.94%, c) 3.85%, d) 5.78% and e) 8.79%, respectively.

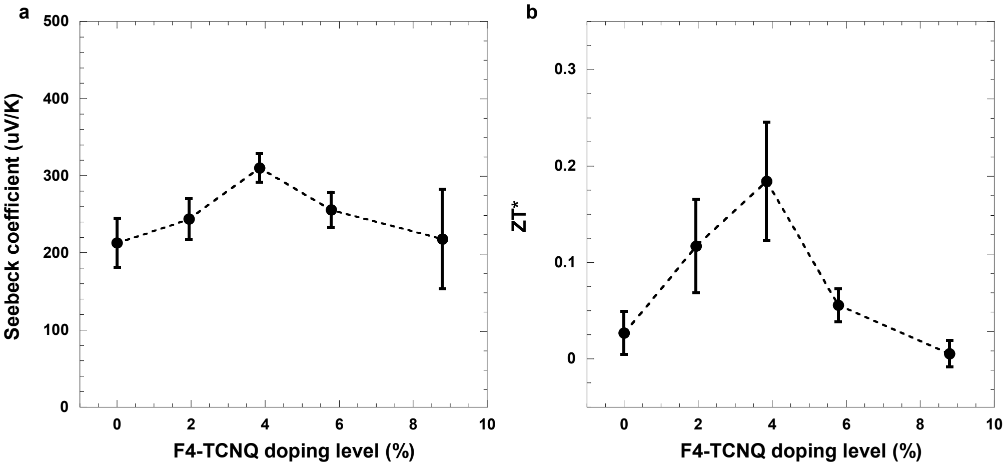

Fig. 6. a) The Seebeck coefficient of the F4-TCNQ doped $FASnI_3$ thin films, and b) the ZT value of the F4-TCNQ doped $FASnI_3$ thin films versus of the doping levels of F4-TCNQ.